Helix−Turn−Helix Peptides That Form α-Helical Fibrils: Turn Sequences Drive Fibril Structure †

ARTICLE *in* BIOCHEMISTRY · OCTOBER 2005

Impact Factor: 3.02 · DOI: 10.1021/bi0509705 · Source: PubMed

5 AUTHORS, INCLUDING:

Kristi Lazar Cantrell
Westmont College
7 PUBLICATIONS **93** CITATIONS
SEE PROFILE

Godfrey S Getz
University of Chicago
256 PUBLICATIONS **8,258** CITATIONS
SEE PROFILE

Joseph P R O Orgel
Illinois Institute of Technology
53 PUBLICATIONS **1,553** CITATIONS
SEE PROFILE

Helix-Turn-Helix Peptides That Form α-Helical Fibrils: Turn Sequences Drive Fibril Structure†

Kristi L. Lazar,‡ Hélène Miller-Auer,§ Godfrey S. Getz,§,|| Joseph P. R. O. Orgel,⊥,+ and Stephen C. Meredith*,§,||

Departments of Chemistry, Pathology, and Biochemistry and Molecular Biology, The University of Chicago, Chicago, Illinois 60637, Department of Biochemistry, Rosalind Franklin University of Medicine and Science, North Chicago, Illinois 60064, and Center for Synchrotron Radiation Research and Instrumentation, Department of Biological, Chemical, and Physical Sciences, Illinois Institute of Technology, Chicago, Illinois 60616

Received May 25, 2005; Revised Manuscript Received July 18, 2005

ABSTRACT: Models of apolipoprotein A-I (apo A-I), the main protein of high-density lipoprotein, predict that it contains 10 amphiphilic, α-helical segments connected by turns. We synthesized four peptides with two identical 18-residue, amphiphilic, α-helical segments (Anantharamaiah, G. M., et al. (1985) *J. Biol. Chem. 260*, 10248−10255) connected by putative turn sequences from apo A-I: (**1**) Ac-DWLKAFYDKVAEKLKEAFKVEPLRADWLKAFYDKVAEKLKEAF-NH_2, (**2**) Ac-DWLKAFYDK-VAEKLKEAFGLLPVLEDWLKAFYDKVAEKLKEAF−NH_2, (**3**) Ac-DWLKAFYDKVAEKLKEAF-KVQPYLDDWLKAFYDKVAEKLKEAF−NH_2, and (**4**) Ac-DWLKAFYDKVAEKLKEAFNGGARLADW-LKAFYDKVAEKLKEAF-NH_2. Surprisingly, peptides **1**−**3** formed fibrils after incubation (37 °C, 10 mM sodium phosphate, pH 7.60), but in contrast to *β*-sheet amyloid fibrils, these did not bind thioflavin T and they induced a blue shift in the spectrum of Congo red. CD (peptides **1**−**3**) and FTIR (peptides **1** and **2**) of the fibrils showed significant α-helical character. Synchrotron X-ray fiber diffraction on a magnetically aligned sample of **1** confirmed the α-helical character in the fibrils and indicated that the helical axes are oriented perpendicular to the fibril axis. In contrast, peptide **4**, containing two Gly residues but no Pro in the turn, formed only a small amount of nonfibrillar precipitate after prolonged incubation. Peptide **4P** (peptide **4** with a Pro in place of the central Ala) and peptide **5**, containing a PEG block in lieu of the central turn, were similar to peptide **4** in not forming fibrils, possibly because the region linking the helices was unstructured. These studies indicate that varying turn sequences between longer amphiphilic α-helical segments can drive the structure of fibrils.

Amyloid fibrils are derived from diverse proteins having little sequence similarity to one another. Despite the lack of homology, these fibrillar aggregates share *β*-sheet-rich secondary structures and have other common features such as appearance by EM[1] and the ability to bind the azo dyes Congo red and thioflavin T (*1*). Amyloid is deposited in tissues in many systemic amyloidoses, and localized deposition of amyloid occurs in neurodegenerative diseases such as Alzheimer's Disease and Huntington's Disease. Recently, Dobson and co-workers have suggested that the extended or *β*-sheet conformation may be the "generic" conformation of the polypeptide chain (*2*, *3*). Fibrils, however, are observed with secondary structures other than the *β*-sheet, and these include the coiled-coil α-helices present in keratin and myosin and the polyproline-II-like helix found in the chains forming the triple helix of collagen (*4*, *5*).

Human apo A-I, the major structural component of human high-density lipoprotein (HDL), is a 243 amino acid protein composed of two major domains (*6*). The first 43 amino acids of apo A-I are nonhelical, while the region comprising amino acids 44−243 is often represented as 10 amphiphilic, α-helical segments of either 22 residues (helices 1, 2, 4−8, and 10) or 11 residues (helices 3 and 9). X-ray crystallography of an N-terminal truncated form of lipid-free human apo A-I (residues 44−243) showed a dimer that formed a continuous ring of α-helical segments (*7*). Many physical

† We thank the NIH Cardiovascular Pathophysiology Training Grant (HL07237 to K.L.L.) and NIH (HL68661 to G.S.G. and NS042852 to S.C.M.) for support of this work. This work benefited from the support of the NSF Research Collaborative Network, 'Fibernet' (MCB-0234001).

* To whom correspondence should be addressed. Department of Pathology, The University of Chicago, 5841 S. Maryland Avenue, Chicago, IL 60637. Tel: 773-702-1267. Fax: 773-834-5251. E-mail: scmeredi@uchicago.edu.

‡ Department of Chemistry, The University of Chicago.

§ Department of Pathology, The University of Chicago.

|| Department of Biochemistry and Molecular Biology, The University of Chicago.

⊥ Rosalind Franklin University of Medicine and Science.

+ Illinois Institute of Technology. Current address for Joseph P. R. O. Orgel.

[1] Abbreviations: A*β*, *β*-amyloid peptide; apo A-I, apolipoprotein A-I.; CD, circular dichroism; DMPC, 1,2-dimyristoyl-*sn*-glycero-3-phosphocholine; DMS, dimethyl sulfide; EDT, ethanedithiol; EM, electron microscopy; ESI, electrospray ionization, Fmoc, 9-fluorenylmethoxycarbonyl; FTIR, Fourier transform infrared spectroscopy; HBTU, 2-(1*H*-benzotriazole-1-yl)-1,1,3,3-tetramethyluronium hexafluorophosphate; HDL, high-density lipoprotein; HOBt, *N*-hydroxybenzotriazole; HPLC, high-performance liquid chromatography; LCAT, lecithin-cholesterol acyltransferase; MALDI-TOF, matrix-assisted laser desorption ionization time-of-flight; MRE, mean residue ellipticity; PEG, poly(ethylene glycol); RP-HPLC, reverse-phase high-performance liquid chromatography; SAA, serum amyloid A; *t*-Boc, *tert*-butyloxycarbonyl; TFA, trifluoroacetic acid.

10.1021/bi0509705 CCC: $30.25
Published on Web 08/30/2005

techniques, such as CD spectroscopy, indicate that this protein also has a high α-helical content in lipid-bound forms. Analysis of apo A-I sequences from many species suggests punctuation of the α-helices by turns, mostly containing a central proline residue. Although these sequences do not form canonical turns in the X-ray structure, the structure of the lipidated protein remains unknown. Several models have been proposed for the arrangement of the α-helical segments of apo A-I in HDL (*6*). A number of short, amphiphilic, α-helical peptides have been shown to recapitulate many of the salient physical properties of the entire apolipoprotein. For example, the 18-residue amphiphilic, α-helical peptide developed by Anantharamaiah and colleagues (referred to as peptide 18A; 18A = Asp-Trp-Leu-Lys-Ala-Phe-Tyr-Asp-Lys-Val-Ala-Glu-Lys-Leu-Lys-Glu-Ala-Phe) binds to lipid, activates lecithin-cholesterol acyltransferase (LCAT), and has other physical and functional properties typical of the full-length protein (*8*, *9*).

Point mutations of apolipoprotein A-I and of other small α-helical apolipoproteins, including apolipoproteins A-II and E, are associated with forms of systemic amyloidosis in humans and mice (*1*, *10*). In addition, serum amyloid A (SAA) is an acute phase reactant that binds to HDL, and in chronic inflammatory diseases, fragments of SAA can be deposited in tissues in a form of systemic amyloidosis (*1*, *10*). In amyloidoses associated with mutant apolipoproteins or SAA, the proteins are believed to undergo an α-helix to *β*-sheet transition concomitant with the formation and deposition of amyloid.

We synthesized a series of helix-turn-helix peptides, in which the helices were two copies of peptide 18A (*8*), and the helices were linked by various native sequences predicted to form turns in human apo A-I. In preliminary studies, we observed the rapid formation of a precipitate in some of them. EM revealed that the precipitates were fibrillar rather than amorphous. Since the two segments linked by the different turn sequences had been optimized specifically as amphiphilic α-helices, and indeed were α-helical when synthesized as single 18 amino acid segments, the question arose whether these fibrils were *β*-sheet amyloids or, on the contrary, whether the self-associating units within the fibrils retained their α-helical structure.

In this paper, we will show that the self-associating units are indeed highly α-helical and show no evidence of *β*-sheet. Furthermore, we will present structural data in support of a novel spatial arrangement of the α-helical segments within the fibril.

EXPERIMENTAL PROCEDURES

Peptide Synthesis and Purification. The peptides were synthesized using standard 9-fluorenylmethoxycarbonyl (Fmoc) and HBTU/HOBt (Fastmoc) solid-phase chemistry on an Applied Biosystems (Foster City, CA) model 431A or 433A peptide synthesizer. All of the peptides were acetylated with acetic anhydride on the synthesizer and amidated with a Fmoc-Rink Amide resin (Anaspec). Peptides were cleaved from the resin using 9 mL of TFA plus 0.5 mL of thioanisole, 0.3 mL of EDT, and 0.2 mL of anisole for 1.5 h at 22 °C. Peptide **5** incorporates PEG segments between two 18A peptide segments. The first 18 amino acids of peptide **5** were synthesized on a MBHA resin (Applied Biosystems) using standard *t*-Boc chemistry, after which the PEG moieties were incorporated by coupling first *tert*-butyloxycarbonyl-11-amino-3,6,9-trioxaundecanoic acid·dicyclohexylamine followed by *tert*-butyloxycarbonyl-8-amino-3,6-dioxaoctanoic acid·dicyclohexylamine (Peptides International). After incorporation of the PEG moieties, the remaining 18 amino acids were incorporated into the peptide using standard *t*-Boc chemistry. The peptide was cleaved from the resin using anhydrous HF in an Immuno-Dynamics (La Jolla, CA) HF apparatus, using 10 mL of HF also containing 1 mL of *p*-cresol and 1 mL of DMS/g of resin for 1 h at −3 to −5 °C. Thus, peptide **5** had the following structure:

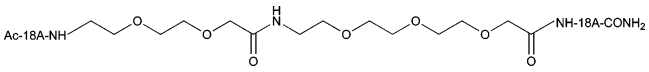

Crude peptides were purified by RP-HPLC on a preparative C18 (Zorbax) column using gradients of water (0.1% v/v TFA) and acetonitrile (0.1% v/v TFA). Peptide purity was greater than 97% by analytical RP-HPLC. The molecular masses of the peptides were verified by ESI and MALDI-TOF mass spectrometry.

Determination of Peptide Concentrations. Peptide concentrations were calculated using the extinction coefficients for the tryptophan and tyrosine residues. The concentrations of peptides **1**, **2**, and **4** in 10 mM sodium phosphate, pH 7.60, were measured (Hitachi U2000 Spectrophotometer) using $\epsilon_{280} = 14\,600\ M^{-1}\ cm^{-1}$, and the concentration of peptide **3** was measured using $\epsilon_{280} = 15\,880\ M^{-1}\ cm^{-1}$ (*11*).

Fibril Sample Preparation. Unless otherwise stated, fibrils were formed by incubating peptides at 37 °C in 10 mM sodium phosphate buffer, pH 7.60. To prepare fibrils, peptides **1**−**3** were incubated at 1 mg/mL and peptide **4** at 2 mg/mL.

Electron Microscopy. Aliquots of fibril samples (5 μL) were applied to a glow-discharged, 400-mesh, carbon-coated support film and stained with 1% uranyl acetate. Micrographs of fibrils were recorded using a FEI Tecnai F30st-STEM Microscope at magnifications of 21 000×, 137 200×, and 343 000×. Aliquots (5 μL) of peptide/DMPC complexes were applied to a glow-discharged, 400-mesh, carbon-coated support film and stained with 2% phosphotungstic acid. Micrographs of peptide/DMPC complexes were recorded at 137 200× and 273 000×. Fibril diameters were measured with the software Digital Micrograph (Gatan, Inc.).

Thioflavin T and Congo Red. Following the formation of fibrils, 10 μL aliquots of the fibrillar peptide were removed and diluted with 1 mL of a 10 μM thioflavin T solution in 10 mM sodium phosphate buffer, pH 7.60. The sample was pipetted vigorously, and the fluorescence was measured (λ_{EX} = 446 nm, λ_{EM} = 490 nm) on a Hitachi F2000 fluorescence spectrophotometer set to a bandwidth of 10 nm and a photomultiplier voltage of 700. After a 3 s delay, the fluorescence was averaged for 10 s. To measure Congo red binding, 3 μL of 0.1% (w/v) Congo red (Sigma) was added to 1 mL of 10 mM sodium phosphate buffer, pH 7.60. The absorbance spectrum was measured from 400 to 600 nm (Hitachi U2000 Spectrophotometer). Approximately 20 μg of fibrillar peptide was added to the Congo red solution and incubated for 20 min at 37 °C. The absorbance spectrum of the dye in the presence of the fibrils was remeasured.

Preparation of 1 mM Large Multilamellar Vesicles of DMPC and Peptide/DMPC Complexes. The procedure described by Mishra et al. was followed to prepare the peptide/lipid complexes (*11*). Briefly, 16.28 mg of DMPC (Avanti Polar Lipids) was dissolved in 1 mL of chloroform in a round-bottom flask. The chloroform was evaporated under a stream of nitrogen followed by evacuation for 30 min to ensure complete evaporation of the organic solvent. Then, a total of 24 mL of 10 mM phosphate buffer, pH 7.60, was added to the solid film. This solution was stirred vigorously at room temperature for 30 min to form a coarse suspension of the lipid in the form of large, multilamellar vesicles. Peptide/DMPC complexes were prepared by adding a freshly dissolved peptide solution to the DMPC suspension, and the mixture was then diluted with 10 mM sodium phosphate, pH 7.60. The final peptide and lipid concentrations were 18 and 360 μM, respectively, to give a peptide/lipid molar ratio of 1:20. The solutions were incubated for 36 h at 22 °C, which resulted in the formation of a clear solution for all of the peptide/lipid complexes.

Far-UV CD of the Peptides and Peptide/DMPC Complexes. CD spectra were collected using an Aviv model 202 CD spectrophotometer (Lakewood, NJ) equipped with a temperature-controlled holder. The CD measurements were collected at intervals of 0.5 nm from 265 to 190 nm with a 1 s averaging time and a 1 nm bandwidth. The CD spectra of freshly dissolved peptide solutions at 1−1.5 μM were measured in 10 mM sodium phosphate, pH 7.60, in 10 mM acetic acid, pH 3.51, and in 1 mM NaOH, pH 11.02. Melting curves for peptides **1**−**4** were measured by heating 1 μM solutions from 20 to 90 °C, at increments of 2 °C. The cuvette was allowed to equilibrate thermally for 1 min at each temperature, after which the ellipticity at 222 nm was measured and averaged for 30 s; the bandwidth was set to 10 nm. CD spectra were also measured of peptide/DMPC complexes in 10 mM sodium phosphate, pH 7.60. The peptide and lipid concentrations were 1.2 and 24 μM, respectively. All spectra were collected in a 1 cm quartz cuvette at 25 °C. Five scans were collected, and the data were averaged and baseline-corrected. The α-helical content of the peptides was estimated from their mean residue ellipticities (MRE) at 222 nm (*12*).

Far-UV CD of Fibril Films. The samples containing fibrils were vortexed, and 40 μL of the resulting slurries were pipetted onto quartz window plates (Starna) cut to the dimensions 12.5 mm × 12 mm × 1.25 mm. The drops were allowed to merge, and the plates were placed in a vacuum desiccator and dried overnight. CD measurements were collected immediately after removing the plates from the desiccator. Thus, the films were dried, and essentially no solvent was present. A baseline was collected after drying 40 μL of 10 mM sodium phosphate, pH 7.60, on the plate. Five scans were collected, and the data were averaged and baseline-corrected. The plate was rotated 90° in the cell holder, and the measurements were repeated to verify the absence of linear dichroism (*13*, *14*).

FTIR of Fibrils. Exchangeable hydrogens in the peptides were replaced by deuterium by dissolving the peptides in D_2O and lyophilizing three times. Fibrils were grown in deuterated 10 mM sodium phosphate, pD 7.60. A 10 μL fibril sample was applied between two CaF_2 plates (International Crystal Laboratories). IR spectra were recorded on a Thermo Nicolet Infrared spectrophotometer equipped with a DTGS-KBr detector. Two hundred interferograms were recorded at room temperature at a resolution of 2 cm^{-1}. The spectrum of 10 μL of deuterated 10 mM sodium phosphate, pD 7.60, was also obtained and subtracted from the fibril spectra.

X-ray Fiber Diffraction. Fibrils of peptide **1** were grown at 37 °C in 10 mM phosphate buffer, pH 7.60. The fibrils were placed in dialysis tubing (Spectra/Por CE MWCO 500) and dialyzed against water to remove the phosphate. The fibril sample was transferred to an eppendorf tube and centrifuged for 30 min at 13 200*g*. The supernatant was removed from the solution, and the fibrils were loaded into a 0.7 mm glass capillary (Charles Supper). To observe the distinction between equatorial and meridional reflections, the capillary was placed inside a 500 MHz NMR for 5 days to achieve partial alignment of the fibrils (*15*, *16*). Synchrotron data were collected at Argonne National Laboratory beamline SER-CAT (bending magnet station) on a marr225 CCD detector, where the X-ray wavelength was 1.00 Å. The sample-to-detector distance was 200 mm. X-ray diffraction data was analyzed with the CCP13 application "FiberFix" (http://www.ccp13.ac.uk/) and FIT2D (http://www.esrf.fr/computing/expg/subgroups/data_analysis/FIT2D/). Background subtraction for Figure 7C was performed using a computer algorithm from the XFIX (FiberFix) program, with the default Roving window settings, and the rotation scan with the "cake" d-scan function of FIT2D.

RESULTS

Peptide Design. The peptides included in these studies were designed to test the role of the putative interhelical turn sequences of apo A-I in modulating binding of this protein to subclasses of HDL. To investigate the role of these turn sequences, we chose to study peptides consisting of two identical, idealized, amphiphilic α-helices, linked by various turn sequences from human apo A-I. Accordingly, we synthesized the following peptides: (**1**) Ac-DWLKAFYDKVAEKLKEAFKVEPLRADWLKAFYDKVAEKLKEAF-NH_2, (**2**) Ac-DWLKAFYDKVAEKLKEAFGLLPVLEDWLKAFYDKVAEKLKEAF-NH_2, (**3**) Ac-DWLKAFYDKVAEKLKEAFKVQPYLDDWLKAFYDKVAEKLKEAF−NH_2, and (**4**) Ac-DWLKAFYDKVAEKLKEAFNGGARLADWLKAFYDKVAEKLKEAF−NH_2.

In all of these peptides, the putative turn sequences (underlined) are flanked on each side by the 18A peptide, designed by Anantharamaiah and colleagues. This peptide has been shown to bind to dimyristoyl lecithin and form bilayer disks in which the peptide is α-helical (*8*). The turn sequences of peptides **1**−**4** above were all selected from human apo A-I, with a length set to be seven amino acids long, and the midpoint defined by the proline residues in those segments that contained a proline. The 18A peptide was designed to be an amphiphilic α-helix, and thus, the inclusion of seven residues between the two helical segments would keep the hydrophobic "faces" of the two helical cylinders in phase, if those seven residues were themselves within an α-helix. The sources of the putative turns are as follows: KVEPLRA = amino acids 118−124, between helices 4 and 5; GLLPVLE = amino acids 217−223, between helices 9 and 10; KVQPYLD = amino acids 96−102, between helices 3 and 4; and NGGARLA = amino acids 185−191, between helices 7 and 8 (*6*).

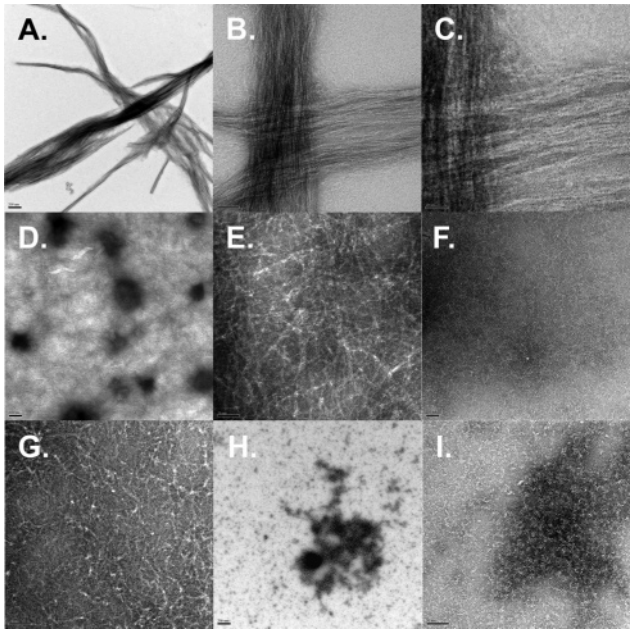

FIGURE 1: Electron micrographs of precipitates formed by peptides **1**−**4**. Fibrils stained with 1% uranyl acetate are shown magnified at 21 000×, 137 200×, and 343 000×, as follows: peptide **1** is shown in panels A, B, and C, at 21 0 00×, 137 200×, and 343 000×, respectively. Peptide **2** is shown in panels D and E at 21 000× and 137 200×, respectively. Peptide **3** is shown in panels F and G at 21 000× and 137 200×, respectively. The amorphous precipitate of peptide **4** is shown in panels H and I at 21 000× and 137 200×, respectively. Panels A, D, F, and H, scale bar = 200 nm. Panels B, E, G, and I, scale bar = 50 nm. Panel C, scale bar = 20 nm.

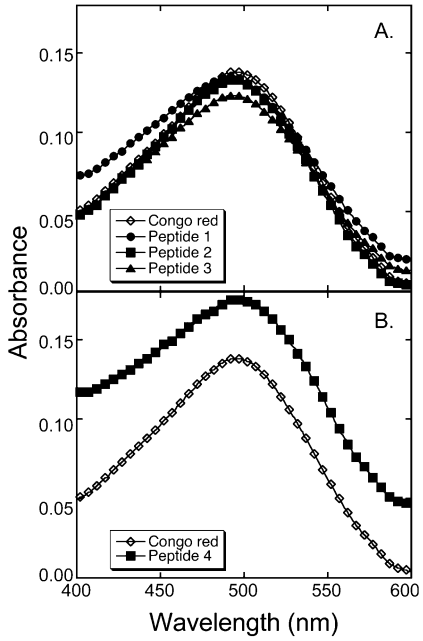

FIGURE 2: Absorbance spectra of Congo red alone, and in combination with slurries of peptide precipitate. Panel A shows fibrils made by peptides **1** (●), **2** (■), and **3** (▲); panel B shows the amorphous precipitate of peptide **4** (■). For clarity, every fifth point is shown.

Formation of Fibrils and Appearance by EM. In initial studies of lipid binding, peptides were first dissolved in 6 M guanidine HCl and 10 mM sodium phosphate, pH 7.60, and then dialyzed against 10 mM sodium phosphate, pH 7.60. We observed that a precipitate formed during the dialysis of peptide **1**, which EM showed to consist of fibrils. We later observed that precipitates could be formed by dissolving and incubating all of the peptides in 10 mM sodium phosphate, pH 7.60, directly.

Peptide **1** formed a precipitate within 1 h (37 °C, 1 mg/mL peptide). The precipitate pelleted into a dense, opaque pellet (13 200 rpm). EM showed discrete linear, unbranched fibrils of ≈3.3 nm diameter that packed laterally into straight tress-like bundles (Figure 1A−C). Peptides **2** and **3** (1 day incubation at 37 °C, 1 mg/mL peptide) formed a large, gel-like, nearly transparent pellet upon centrifugation (13 200 rpm). Electron micrographs of **2** showed individual fibrils of ≈3.3 nm diameter which tended to pack into doublets of ≈7.0 nm diameter (Figure 1D,E). Electron micrographs of **3** were similar to those of peptide **1**, showing linear, unbranched fibrils of ≈3.3 nm diameter with significant lateral association (Figure 1F,G). Peptide **4** yielded only a small amount of precipitate after incubation in the same buffer at 2 mg/mL for 30 days at 37 °C. EM showed that the precipitate was nonfibrillar (Figure 1H,I).

For all peptides that formed fibrils readily at pH 7.60, no precipitate formed when the peptides were dissolved into a solution at pH 3.51 (10 mM acetic acid) or pH 11.02 (1 mM NaOH). Fibrils of **1** could also be formed by dissolving the peptide at 1 mg/mL in 10 mM sodium phosphate, pH 7.60, also containing either 4 M NaCl or 3 M urea. The fibril appearances by EM were not distinguishable from fibrils formed in the absence of 4 M NaCl or 3 M urea.

Thioflavin T and Congo Red. The β-sheet fibrils referred to as amyloids typically bind azo dyes such as thioflavin T and Congo red. Binding of thioflavin T to amyloids leads to characteristic fluorescence (λ_{ex} = 446 nm, λ_{em} = 490 nm), while binding of Congo red to amyloids leads to a red-shift of the absorbance spectrum (*17*). By these criteria, the fibrils formed by peptides **1**−**3** were not amyloids. None of these peptides induced thioflavin T fluorescence. After incubation of the peptides in buffer for at least three weeks, thioflavin fluorescence values for peptides **1**, **2**, and **3** were 1.1, 3.5 and 3.5 above background, respectively; for comparison, Aβ_{1-40} fibrils gave values of ≈100. Peptides **1**, **2**, and **3** all caused a slight blue-shift (0.5−1.0 nm) in the λ_{max} of the Congo red absorption spectrum (Figure 2A). We observed a red-shift in λ_{max} from 499 to 510 nm with amyloid fibrils derived from Aβ_{1-40} (data not shown).

In contrast to peptides **1**−**3**, the small amount of precipitate obtained from peptide **4** induced an increase in thioflavin T fluorescence, with a value of 96.1, that is, similar to those of Aβ_{1-40} fibrils. Peptide **4** also caused a slight red-shift in the λ_{max} of the Congo red spectrum (Figure 2B). This is characteristic of amyloid fibrils, although fibrillar structure was not observed by EM (Figure 1H,I).

CD Spectra of Peptides in Solution and in Association with Phospholipid Bilayer Disks. Far-UV CD spectroscopy of the peptides in solution shows α-helical structure (Figure 3A). Initial experiments indicated that peptide **1** was the least soluble of the four peptides and formed fibrils at concentrations >1 μM (10 mM sodium phosphate, pH 7.60). Although higher concentrations of the peptide appeared to go into solution, after a brief incubation at 22 or 37 °C, a precipitate formed, leaving a final peptide concentration of ≈1 μM. Consequently, to compare the four peptides, CD spectra were

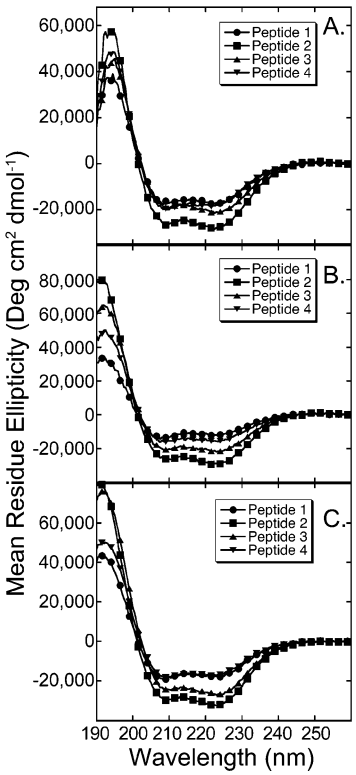

FIGURE 3: CD spectra of peptides **1**−**4** in buffer. Panel A shows 1−1.5 μM peptide solutions in 10 mM sodium phosphate, pH 7.60: peptide **1** (●), **2** (■), **3** (▲), and **4** (▼). Panels B and C are the CD spectra of peptides **1**−**4** in 10 mM acetic acid, pH 3.51, and 1 mM NaOH, pH 11.02, respectively: peptide **1** (●), **2** (■), **3** (▲), and **4** (▼). For clarity, every fifth point is shown.

measured with peptide concentrations of 1−1.5 μM. The CD spectra of the four peptides show prominent minima at 208 and 222 nm, and the spectra cross the abscissa at ≈203 nm, consistent with significant α-helical character of these peptides in solution. The helical content of the peptides was estimated from their mean residue ellipticities at 222 nm (*12*). The helical contents of peptides **1**−**4** were 52, 79, 69, and 54%, respectively. Although precipitates or fibrils did not form when the peptides were dissolved in 10 mM acetic acid (pH 3.51) or 1 mM NaOH (pH 11.02), the α-helical character of these peptides was maintained in CD spectra (Figure 3, panels B and C, respectively). In addition, melting curves demonstrated noncooperative transitions, with midpoints at ≈60 °C, consistent with progressive fraying of α-helices (Figure 4). In contrast, a coiled-coil α-helical peptide, such as GCN4-p1, would show a cooperative melt, consistent with a two-state equilibrium (*18*).

All of the peptides formed discoidal bilayers when incubated (1.5 days, 37 °C) with coarse suspensions of DMPC as large multilamellar vesicles (Figure 5A). Similar results have been observed in studies of peptides 18A and 18A-P-18A (where the P is a proline interposed between the helices) with DMPC (*8*). The far-UV CD spectra of 1.2 μM peptides in the presence of 24 μM DMPC are shown in Figure 5B. These spectra are qualitatively similar to those of the peptides in the absence of lipid, but the α-helical contents of peptides **1**−**4** in the presence of DMPC were 64, 79, 74, and 79%, respectively. Thus, peptides **1**, **3**, and **4** showed increases in apparent α-helical content in the presence of DMPC, while peptide **2**, the peptide with the highest α-helical content in the absence of lipid, showed essentially no change.

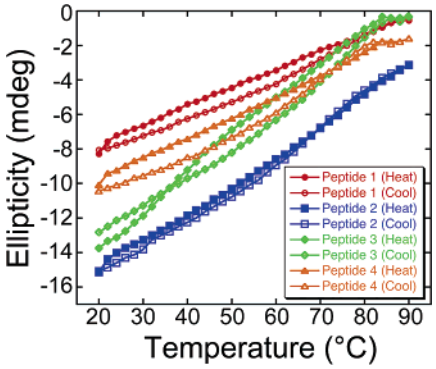

FIGURE 4: Thermal melts of 1 μM solutions of peptides **1**−**4**. Peptides were heated from 20 to 90 °C, at increments of 2 °C. The cuvette was allowed to equilibrate thermally for one minute at each temperature, after which the ellipticity at 222 nm was measured and averaged for 30 s. Curves for heating and cooling were measured sequentially and are given separate symbols.

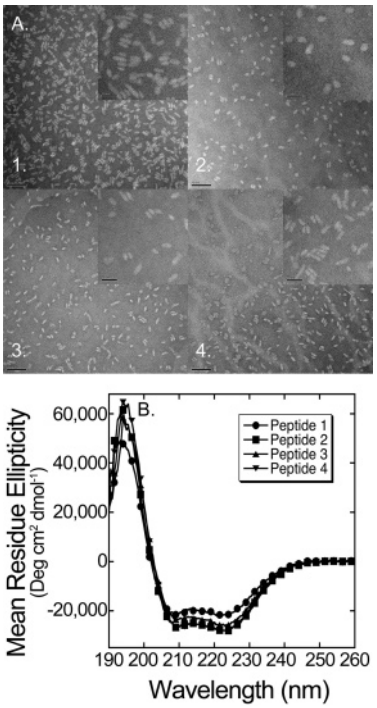

FIGURE 5: (A) Electron micrographs of peptides **1**−**4** in the presence of DMPC bilayers (peptide/DMPC = 1/20, mole/mole) stained with 2% phosphotungstic acid at 137 200× (inset: 273 000×); the peptides formed disks that, in some cases, stacked. Scale bar = 50 nm (Inset: scale bar = 20 nm). (B) CD spectra of the peptides in the presence of DMPC: peptide **1** (●), **2** (■), **3** (▲), and **4** (▼). For clarity, every fifth point is shown.

In contrast to 18A, which binds to lipids with high affinity in many assays (*8*), we could demonstrate lipid binding by our peptides only in the above DMPC clarification assay. We did not observe lipid binding in other lipid binding assays, for example, changes in CD or intrinsic tryptophan fluorescence in the presence of 1000 Å diameter single bilayer DMPC vesicles (data not shown).

*CD of Fibrils from Peptides **1**−**3***. The secondary structure of fibrils of peptides **1**−**3** was investigated using CD spectroscopy of fibril films on quartz plates. Because of variations in the thickness of the films, we sought to normalize the CD spectrum to allow comparison of the

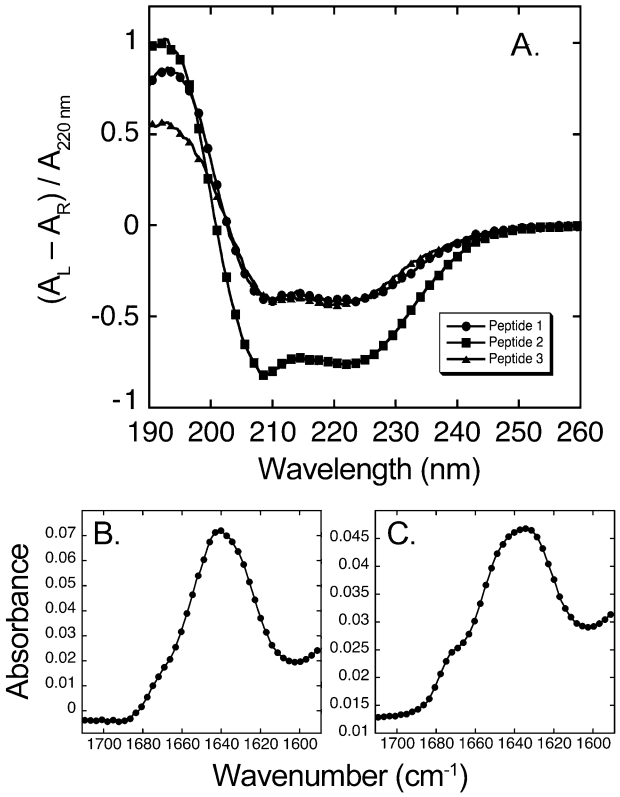

FIGURE 6: CD and FTIR spectra of peptide fibrils. Panel A shows CD spectra of fibrils of peptides **1**−**3**. Panels B and C show FTIR spectra in the amide I' region recorded for fibrils from peptides **1** and **2**, respectively. For clarity, every third point is shown.

different peptides. Accordingly, when a variation of the technique of McPhie is used (*13*, *14*), Figure 6A shows the CD signal (as $A_L - A_R$) divided by the absorbance of the film at a convenient wavelength (220 nm) as a surrogate for the concentration of the peptide in the film. The CD spectra show prominent minima at 208 and 222 nm, and they cross the abscissa at ≈203 nm, consistent with significant α-helical character in the fibrils. Attempts to measure CD spectra of precipitates of peptide **4** yielded no measurable ellipticity (data not shown).

*FTIR of Fibrils from Peptides **1** and **2***. FTIR confirmed the findings obtained by CD spectroscopy. FTIR spectra of the fibrils from peptides **1** and **2** showed amide I' bands with maxima at 1641 and 1633 cm^{-1}, respectively (Figure 6, panels B and C, respectively). The band at 1641 cm^{-1} is consistent with α-helical structure (*19*). While the band at 1633 cm^{-1} is somewhat lower than that observed for most α-helical peptides, this has been reported for coiled-coil α-helices, which can show an amide I' band at a frequency as low as 1630 cm^{-1} (*20*, *21*). *β*-sheet amyloids typically produce amide I' bands with maxima at ≈1620 cm^{-1} (*22*).

*Synchrotron X-ray Fiber Diffraction on Partially Aligned Fibrils of **1***. Fibrils of peptide **1** were placed in a 500 MHz NMR for 5 days to achieve partial alignment of the fibrils. At the end of this period, the fibrils formed a band with the longitudinal axis perpendicular to the long axis of the capillary tube. The orientation of the fibrils was determined by inspection of the fibrils by light and electron microscopy. By light microscopy, we were able to observe the macroscopic orientation of the fibers. Electron microscopy also demonstrated that these fibers were composed of compacted

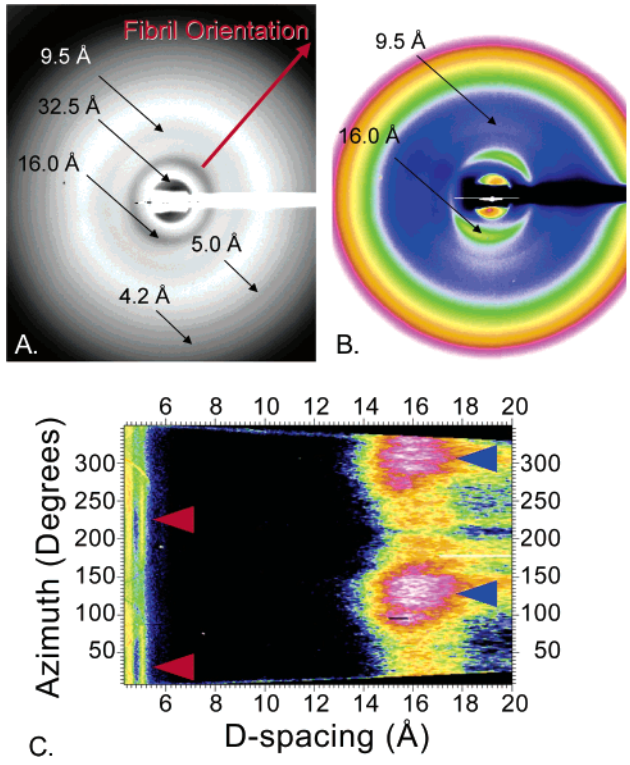

FIGURE 7: X-ray fiber diffraction pattern of partially aligned fibrils of peptide **1**. (A) The approximate fibril axis is shown by the arrow in the figure. Meridional reflections are at 9.5 and 16.0 Å, and equatorial reflections are at 4.2 and 5.0 Å. Additional reflections are present at 1.55 (not shown) and 32.5 Å, but the orientation of these reflections could not be determined. The relative orientations of the 4.2, 5.0, and 16.0 Å reflections are clearly discernible. Panel B shows the low angle part of the diffraction pattern in the same orientation as in panel A. The image is pseudocolored and the maximum of the intensity scale threshold lowered to help identify the orientation of the 9.5 and 16.0 Å reflections, which obscures the relative orientation of the 5.0 and 4.2 Å reflections. Panel C shows a rotational D-space scan of the data shown in panels A and B. In Panel C (same color scale as B), the D-spacings are plotted as a function of the azimuthal angle; 0° is defined arbitrarily as the 3 o'clock position in panels A and B. The figure is also background-subtracted, so that the 5.0 and 16.0 Å reflections can be seen at the same time on this scale using the CCP13 XFIX (FiberFix) program. The figure shows that the intensity distribution of the 5.0 (red arrowheads) and 16.0 Å (blue arrowheads) reflections are perpendicular to one another.

bundles of fibrils with the same orientation as the larger fibers (Figure 1A−C). Accordingly, we assumed that the orientation of the fibrils in the X-ray diffraction sample was that of the fibers. The X-ray diffraction pattern of these fibrils is shown in Figure 7. Meridional reflections were observed at 9.5 and 16.0 Å, and equatorial reflections were observed at 4.2 and 5.0 Å. Additional reflections were observed at 1.55 and 32.5 Å. We were unable to determine the orientation of these reflections due to limitations in the experimental setup (obscured by backstop/edge of the detector). To demonstrate clearly the orientation of the 9.5 and 16.0 Å reflections, the data shown in Figure 7A was replotted as a pseudocolored figure (Figure 7B). In addition, Figure 7C shows a D-space scan of the data shown in Figure 7B, that is, in which the D-spacings are plotted as a function of the azimuthal angle. The figure clearly demonstrates that the 5.0 Å reflection is perpendicular to the 16.0 Å reflection.

*Model of Peptide **1** Fibrils*. Based on CD, FTIR, and, most importantly, X-ray diffraction data, we have proposed a

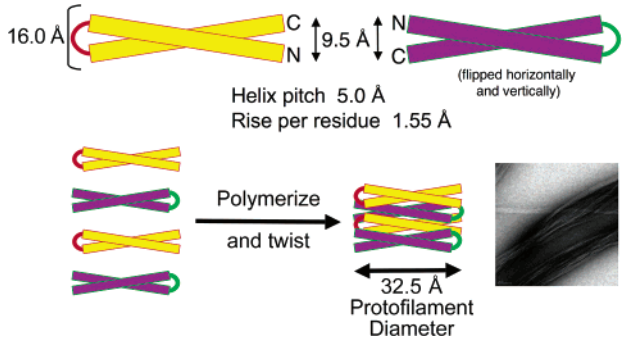

FIGURE 8: Model of peptide **1** fibril. In the proposed model, the α-helical axes are perpendicular to the long axis of the fibril. The 5.0 Å reflection corresponds to the pitch of the α-helices. The 9.5 Å reflection represents the mean distance between the axes of adjacent α-helices. The 16.0 Å reflection is the diameter of a dimer of α-helices. The reflection at 1.55 Å may represent the rise per residue within the individual α-helix. The reflection at 32.5 Å is in experimental agreement with the diameter of the individual fibril ("protofilament") as measured from EM.

structural model of fibrils made from peptide **1** (Figure 8). Meridional reflections are oriented along the fibril axis, whereas equatorial reflections indicate structural spacings perpendicular to the main fibril axis. The 5.0 Å reflection corresponds to the pitch of the α-helices, and this equatorial reflection would place the axis of the helices perpendicular to the fibril axis. Thus, the partial alignment of the fibrils by a magnetic field positions the α-helical axes parallel to the capillary long axis, possibly due to a dipole of the side chains of the α-helical segments. According to the model, the 9.5 Å reflection represents the mean distance between the axes of adjacent α-helices. The 16.0 Å reflection falls within the range of expected values for the diameter of a dimer of α-helices. Although the orientation of the reflection at 1.55 Å could not be determined, it is attributed to the rise per residue within the individual α-helix. The additional reflection at 32.5 Å agrees within experimental limits with the diameter of the individual fibril as measured from EM. Electron micrographs of the fibrils at 343 000× magnification suggest a spiral shape of the fibril (Figure 1C) and show a mean diameter of ≈32.5 Å.

*Additional Peptides To Examine the Difference between Peptide **4** and Peptides **1**−**3**.* The above data indicate that peptides **1**−**3** form fibrils with prominent α-helical character, while peptide **4**, though α-helical in solution and when bound to DMPC disks, did not form fibrils. One possible cause of the difference between peptide **4** and the others in these studies is that only peptide **4** lacks a proline in its putative turn sequence. To examine whether a central proline would be sufficient to allow peptide **4** to form fibrils similar to those of peptides **1**−**3**, we synthesized peptide **4P** with a Pro replacing the central Ala of peptide **4**: (**4P**) Ac-DWLKAFY-DKVAEKLKEAFNGGPRLADWLKAFYDKVAEKLKEAF-NH_2.

Peptide **4P**, like peptide **4**, did not form fibrils. Electron micrographs of a small amount of precipitate obtained after two weeks of incubation at 37 °C showed amorphous deposits rather than fibrils (Figure 9A,B). The peptide induced thioflavin T fluorescence, giving a value of 37.6, somewhat elevated, though not quite as much as peptide **4**. CD of peptide **4P** at 1.2 μM in 10 mM sodium phosphate, pH 7.60, was similar to those of peptide **4** (Figure 9E); from $MRE_{222\ nm}$ the α-helical content was estimated to be 40%.

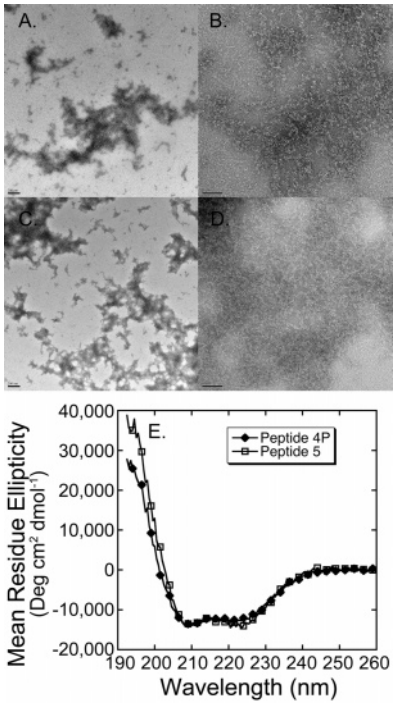

FIGURE 9: (A and B) Electron micrographs of precipitates formed by peptide **4P**, stained with 1% uranyl acetate, and shown magnified at 21 000× and 137 200×, respectively. (C and D) Electron micrographs of precipitates formed by peptide **5**, stained with 1% uranyl acetate, and shown magnified at 21 000× and 137 200×, respectively. Panels A and C, scale bar = 200 nm. Panels B and D, scale bar = 50 nm. (E) CD spectra of peptides **4P** (◆) and **5** (□) in buffer; both peptides are at 1.2 μM, in 10 mM sodium phosphate, pH 7.60. For clarity, every fifth point is shown.

We also synthesized peptide **5**, in which the amino acids of the putative turn segment were replaced by a PEG linker to give a highly flexible segment with the same number of backbone covalent bonds as the other peptides:

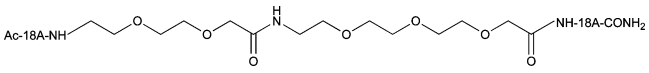

Like peptides **4** and **4P**, peptide **5** formed only a small amount of precipitate after prolonged incubation, and by EM, this did not appear to be fibrillar (Figure 9C,D). CD of the peptide (Figure 9E) showed prominent α-helical structure, with an α-helical content estimated to be 44%.

DISCUSSION

In this paper, we have shown that a helix-turn-helix peptide containing an interhelical region from human apo A-I flanking two identical, idealized, amphiphilic α-helical segments forms fibrils with a novel structure. To our knowledge, this is the first example of peptides forming α-helical fibrils with the α-helices oriented perpendicular to the fibril axis. These studies were part of a comparison of four such helix-turn-helix peptides, all containing two copies of identical α-helical segments, differing only in the sequence of the putative turns. Our data indicate that, in this series of peptides, the turn sequence determines whether the peptide will form fibrils and governs the secondary structure present in those fibrils. Peptides **1**−**3** formed α-helical fibrils, while peptide **4** did not form fibrils under the conditions tested. Peptide **4** is notable both for containing two Gly

residues in the putative turn region and for lacking a Pro residue, which is at the center of the turn region of the other peptides. Peptide **4P**, however, also did not form fibrils, despite the substitution of a Pro for the Ala in the central position of the putative turn in peptide **4**. The appearances in electron micrographs of precipitates formed by peptides **4** and **4P** and their CD spectra were quite similar to those of peptide **5**, which had a PEG segment inserted in lieu of amino acids between the two 18A sequences. The similarity of peptides **4**, **4P**, and **5** suggests that the region linking the two 18A segments in peptide **4** is largely flexible and unstructured.

Peptide **1** formed α-helical fibrils rapidly and had the lowest solubility of the four peptides. Fibril formation was not prevented by dissolving the peptide in 3 M urea but was prevented by raising the pH to 11.0 or lowering the pH to 3.5. These results suggest that electrostatic interactions may be important in the fine structure of the turn region. Fibrils also formed in the presence of 4 M NaCl, but high-salt concentrations both abrogate ionic interactions and increase hydrophobic interactions. The turn region of peptide **1** contains three charged residues placed so that, at pH close to neutrality, oppositely charged groups can interact with one another; that is, in the sequence KVEPLRAD, E and R could interact, while K could interact with the D that begins the C-terminal α-helix. At the same time, the noncooperative melting behavior of peptide **1** at low concentrations, at which the peptide is mainly monomer, suggests that the two α-helical segments of a single peptide molecule do not form a coiled-coil and do not significantly interact with each other. Rather, the noncooperative melt suggests progressive fraying of the α-helix, as is typical for peptides comprised of a single α-helical segment.

Amyloidoses are characterized by the aggregation and deposition of proteins or peptides, all having in common the "cross-β" structure. It is possible that virtually any protein can form amyloid under the appropriate conditions (*2*, *3*). For example, amyloid fibrils have been formed in vitro from myoglobin and homopolymers of polythreonine and polylysine (*23*, *24*). A recent count of proteins associated with amyloid diseases, at 21 different proteins, is certainly an underestimate of the total (*1*). These proteins have no sequence or obvious structural similarity other than forming amyloid. Among these proteins are point mutants of apolipoproteins A-I, A-II, and E, as well as fragments of an acute phase apolipoprotein, the serum amyloid A protein, fragments of which are deposited in tissues as β-sheet-rich fibrils in Amyloid A (AA) amyloidosis (*1*, *10*). Ordered helical structure has been observed in ex vivo amyloid fibrils derived from an apo A-I Leu174Ser variant (*25*). The X-ray fiber diffraction pattern from partially aligned fibrils shows the "cross-β" pattern characteristic of amyloid, although residual ordered α-helical structure was also observed with the α-helices oriented perpendicular to the main fibril axis.

α-Helical fibrils appear to be uncommon, but within the past decade, there has been a small number of proposed α-helical fibrils assembled from synthetic peptides with 21−42 residues (*26*−*30*). All of these examples are based on fibrils with coiled-coils extending along the fibril axis and, thus, appear to differ from the fibrils discussed in this paper. In addition to synthetic peptides, the paired helical filaments of the protein tau and one aggregated form of the yeast prion protein Ure2p have also been proposed to aggregate through α-helical domains, though this remains controversial (*31*, *32*). Another possible example of an α-helical fibril may be lithostathine. Lithostathine fibrils have been found in the pathological lesions of Alzheimer's disease and in the amyloid plaques formed from prion protein in Creutzfeldt-Jakob and Gerstmann-Sträussler-Scheinker diseases. Lithostathine fibrils, like those reported for peptides **1**−**3**, induce a small blue-shift in the spectrum of Congo red (*33*).

Our data support the idea that fibrillar aggregation is a widespread phenomenon that is not restricted to β-sheet-forming peptides and appears to be possible in any repetitive structural element and, hence, any secondary structural unit. Two other principles highlighted by our data may be widely applicable to other types of fibril-forming peptides. First, in this series of peptides based on the 18A amphiphilic α-helix, lipid−protein interactions appear to compete with protein−protein interactions. While 18A itself binds to lipids with high affinity, we could demonstrate lipid binding by our peptides only in a DMPC clarification assay. Similarly, others have reported that for β-amyloid, islet amyloid polypeptide, and α-synuclein lipid binding can abrogate fibril formation, and vice versa (*34*−*37*). Second, while fibrils in general (and possibly amyloid fibrils in particular) might be a "default" or "generic" conformation of polypeptide chains, much effort has gone into the search for intrinsic secondary structural propensities that could promote fibril formation. Our data indicate that intrinsic structural propensities must be weighed against the context in which secondary structures occur. For the peptides considered herein, the intrinsic structural propensities of the 18A segments are identical by definition, and structural differences must be attributed to the context of the sequences connecting these secondary structural elements.

ACKNOWLEDGMENT

We thank Dr. Mohammed Yousef (Biophysical Core Facility), Dr. Josh Kurutz (NMR Facility), Yimei Chen (Electron Microscopy Facility), and Drs. Giridher Reddy and Chang-Jin Qin (Mass Spectrometry Facilities) at The University of Chicago. Dr. Tobin Sosnick and Dr. Wouter Hoff provided assistance with the CD and FTIR experiments, and Dr. Phoebe Rice provided assistance with the X-ray diffraction studies (The University of Chicago). Dr. Gerald Stubbs and Amy Kendall (Vanderbilt University) offered help with sample preparation for the diffraction studies. Data were collected at the Southeast Regional Collaborative Access Team (SER-CAT) 22-BM beamline at the Advanced Photon Source, Argonne National Laboratory. Supporting institutions can be found at www.ser-cat.org/members.html. Use of the Advanced Photon Source was supported by the U.S. Department of Energy, Office of Science, Office of Basic Energy Sciences, under Contract No. W-31-109-Eng-38. We thank the staff of the BioCAT (supported by NIH No. RR-08630), SBC-CAT BM (supported by DOE No. W-31-109-ENG-38), and SER-CAT beamlines for their assistance in the development of this project.

REFERENCES

1. Merlini, G., and Bellotti, V. (2003) Molecular mechanisms of amyloidosis, *N. Engl. J. Med. 349*, 583−596.

2. Dobson, C. M. (2001) The structural basis of protein folding and its links with human disease, *Philos. Trans. R. Soc. London, Ser. B 356*, 133−145.
3. Dobson, C. M. (1999) Protein misfolding, evolution and disease, *Trends Biochem. Sci. 24*, 329−332.
4. Cohen, C., and Parry, D. A. D. (1986) α-Helical coiled coils—a widespread motif in proteins, *Trends Biochem. Sci. 11*, 245−248.
5. Ramachandran, G. N. (1988) Stereochemistry of collagen, *Int. J. Pept. Protein Res. 31*, 1−16.
6. Brouillette, C. G., Anantharamaiah, G. M., Engler, J. A., and Borhani, D. W. (2001) Structural models of human apolipoprotein A-I: a critical analysis and review, *Biochim. Biophys. Acta 1531*, 4−46.
7. Borhani, D. W., Rogers, D. P., Engler, J. A., and Brouillette, C. G. (1997) Crystal structure of truncated human apolipoprotein A-I suggests a lipid-bound conformation, *Proc. Natl. Acad. Sci. U.S.A. 94*, 12291−12296.
8. Anantharamaiah, G. M., Jones, J. L., Brouillette, C. G., Schmidt, C. F., Chung, B. H., Hughes, T. A., Bhown, A. S., and Segrest, J. P. (1985) Studies of synthetic peptide analogs of the amphipathic helix—structure of complexes with dimyristoyl phosphatidylcholine, *J. Biol. Chem. 260*, 10248−10255.
9. Chung, B. H., Anantharamaiah, G. M., Brouillette, C. G., Nishida, T., and Segrest, J. P. (1985) Studies of synthetic peptide analogs of the amphipathic helix—correlation of structure with function, *J. Biol. Chem. 260*, 10256−10262.
10. Hatters, D. M., and Howlett, G. J. (2002) The structural basis for amyloid formation by plasma apolipoproteins: a review, *Eur. Biophys. J. 31*, 2−8.
11. Mishra, V. K., Palgunachari, M. N., Lund-Katz, S., Phillips, M. C., Segrest, J. P., and Anantharamaiah, G. M. (1995) Effect of the arrangement of tandem repeating units of class A amphipathic α-helixes on lipid interaction, *J. Biol. Chem. 270*, 1602−1611.
12. Morrisett, J. D., David, J. S. K., Pownall, H. J., and Gotto, A. M., Jr. (1973) Interaction of an apolipoprotein (ApoLP-alanine) with phosphatidylcholine, *Biochemistry 12*, 1290−1299.
13. McPhie, P. (2001) Circular dichroism studies on proteins in films and in solution: estimation of secondary structure by g-factor analysis, *Anal. Biochem. 293*, 109−119.
14. McPhie, P. (2004) CD studies on films of amyloid proteins and polypeptides: quantitative g-factor analysis indicates a common folding motif, *Biopolymers 75*, 140−147.
15. Stubbs, G. (1999) Developments in fiber diffraction, *Curr. Opin. Struct. Biol. 9*, 615−619.
16. Torbet, J. (1987) Using magnetic orientation to study structure and assembly, *Trends Biochem. Sci. 12*, 327−330.
17. Klunk, W. E., Jacob, R. F., and Mason, R. P. (1999) Quantifying amyloid by Congo red spectral shift assay, *Methods Enzymol. 309*, 285−305.
18. O'Shea, E. K., Rutkowski, R., and Kim, P. S. (1989) Evidence that the leucine zipper is a coiled coil, *Science 243*, 538−542.
19. Haris, P. I., and Chapman, D. (1995) The conformational analysis of peptides using Fourier transform IR spectroscopy, *Biopolymers 37*, 251−263.
20. Reisdorf, W. C., Jr., and Krimm, S. (1996) Infrared amide I' band of the coiled coil, *Biochemistry 35*, 1383−1386.
21. Heimburg, T., Schünemann, J., Weber, K., and Geisler, N. (1999) FTIR-spectroscopy of multistranded coiled coil proteins, *Biochemistry 38*, 12727−12734.
22. Fink, A. L. (1998) Protein aggregation: folding aggregates, inclusion bodies and amyloid, *Folding Des. 3*, R9−23.
23. Fändrich, M., Fletcher, M. A., and Dobson, C. M. (2001) Amyloid fibrils from muscle myoglobin, *Nature 410*, 165−166.
24. Fändrich, M., and Dobson, C. M. (2002) The behaviour of polyamino acids reveals an inverse side chain effect in amyloid structure formation, *EMBO J. 21*, 5682−5690.
25. Mangione, P., Sunde, M., Giorgetti, S., Stoppini, M., Esposito, G., Gianelli, L., Obici, L., Asti, L., Andreola, A., and Viglino, P., et al. (2001) Amyloid fibrils derived from the apolipoprotein A1 Leu174Ser variant contain elements of ordered helical structure, *Protein Sci. 10*, 187−199.
26. Pandya, M. J., Spooner, G. M., Sunde, M., Thorpe, J. R., Rodger, A., and Woolfson, D. N. (2000) Sticky-end assembly of a designed peptide fiber provides insight into protein fibrillogenesis, *Biochemistry 39*, 8728−8734.
27. Ogihara, N. L., Ghirlanda, G., Bryson, J. W., Gingery, M., DeGrado, W. F., and Eisenberg, D. (2001) Design of three-dimensional domain-swapped dimers and fibrous oligomers, *Proc. Natl. Acad. Sci. U.S.A. 98*, 1404−1409.
28. Potekhin, S. A., Melnik, T. N., Popov, V., Lanina, N. F., Vazina, A. A., Rigler, P., Verdini, A. S., Corradin, G., and Kajava, A. V. (2001) De novo design of fibrils made of short α-helical coiled coil peptides, *Chem. Biol. 8*, 1025−1032.
29. Ryadnov, M. G., and Woolfson, D. N. (2003) Engineering the morphology of a self-assembling protein fibre, *Nat. Mater. 2*, 329−332.
30. Zimenkov, Y., Conticello, V. P., Guo, L., and Thiyagarajan, P. (2004) Rational design of a nanoscale helical scaffold derived from self-assembly of a dimeric coiled coil motif, *Tetrahedron 60*, 7237−7246.
31. Sadqi, M., Hernández, F., Pan, U.-M., Pérez, M., Schaeberle, M. D., Ávila, J., and Muñoz, V. (2002) α-Helix structure in Alzheimer's disease aggregates of tau-protein, *Biochemistry 41*, 7150−7155.
32. Bousset, L., Briki, F., Doucet, J., and Melki, R. (2003) The native-like conformation of Ure2p in fibrils assembled under physiologically relevant conditions switches to an amyloid-like conformation upon heat-treatment of the fibrils, *J. Struct. Biol. 141*, 132−142.
33. Laurine, E., Grégoire, C., Fändrich, M., Engemann, S., Marchal, S., Thion, L., Mohr, M., Monsarrat, B., Michel, B., and Dobson, C. M., et al. (2003) Lithostathine quadruple-helical filaments form Proteinase K-resistant deposits in Creutzfeldt-Jakob disease, *J. Biol. Chem. 278*, 51770−51778.
34. Tashima, Y., Oe, R., Lee, S., Sugihara, G., Chambers, E. J., Takahashi, M., and Yamada, T. (2004) The effect of cholesterol and monosialoganglioside (GM1) on the release and aggregation of amyloid *β*-peptide from liposomes prepared from brain membrane-like lipids, *J. Biol. Chem. 279*, 17587−17595.
35. Kurganov, B., Doh, M., and Arispe, N. (2004) Aggregation of liposomes induced by the toxic peptides Alzheimer's A*β*s, human amylin and prion (106-126): facilitation by membrane-bound G_{M1} ganglioside, *Peptides 25*, 217−232.
36. Knight, J. D., and Miranker, A. D. (2004) Phospholipid catalysis of diabetic amyloid assembly, *J. Mol. Biol. 341*, 1175−1187.
37. Zhu, M., and Fink, A. L. (2003) Lipid binding inhibits α-synuclein fibril formation, *J. Biol. Chem. 278*, 16873−16877.

BI0509705